

The load-response of the flagellar beat (accepted for publication in *Phys. Rev. Lett.*)

Gary S. Klindt,¹ Christian Ruloff,² Christian Wagner,^{2,3} and Benjamin M. Friedrich^{1,4,*}

¹*Max Planck Institute for the Physics of Complex Systems, Dresden, Germany*

²*Experimental Physics, University of the Saarland, Saarbrücken, Germany*

³*Physics and Materials Science Research Unit, University of Luxembourg, Luxembourg, Luxembourg*

⁴*Center for Advancing Electronics Dresden cfaed, TU Dresden, Dresden, Germany*

(Dated: February 11, 2022)

Cilia and flagella exhibit regular bending waves that perform mechanical work on the surrounding fluid, to propel cellular swimmers and pump fluids inside organisms. Here, we quantify a force-velocity relationship of the beating flagellum, by exposing flagellated *Chlamydomonas* cells to controlled microfluidic flows. A simple theory of flagellar limit-cycle oscillations, calibrated by measurements in the absence of flow, reproduces this relationship quantitatively. We derive a link between the energy efficiency of the flagellar beat and its ability to synchronize to oscillatory flows.

PACS numbers: 87.16.Qp, 47.63.-b, 05.45.Xt

Keywords: flagellum, cilium, microfluidics, low Reynolds number, active oscillator, synchronization

Introduction. Motile cilia and flagella are slender cell appendages of length $10 - 100 \mu\text{m}$ that exhibit regular bending waves with typical frequencies of $10 - 100 \text{ Hz}$ [1], rendering the beating flagellum a prime example of a micro-mechanical oscillator. The flagellar beat propels eukaryotic microswimmers in a liquid, including sperm cells, non-bacterial pathogens, and green alga. In the human body, self-organized metachronal waves of short flagella termed cilia transport fluids, *e.g.* mucus in the airways [2] and cerebrospinal fluid in the brain [3]. The cytoskeletal core of cilia and flagella, the axoneme, was highly conserved in evolution, from protists to plants and animals [4].

Flagellar bending waves arise by a dynamic instability in the collective dynamics of $10^4 - 10^5$ molecular dynein motors, which are regularly spaced along the flagellar axoneme [5]. This motor activity empowers the eukaryotic flagellum to exert active forces on the surrounding liquid and to set it in motion. Conversely, hydrodynamic friction forces acting along the flagellum feedback on its motor dynamics and change speed and shape of the flagellar beat. Previous research reported a decrease of wave amplitude and frequency in swimming medium of increased viscosity [6, 7]. A force-velocity relationship of the flagellar beat for a time-varying load has been measured in a swimming alga by exploiting rotational self-motion of the cell [8]. Additionally, external fluid flow can perturb the shape of the beat [9]. These experiments indicate an intricate flagellar load-response, which represents a cell-scale counterpart of the known force-velocity relations of individual molecular motors [10] or the torque-speed relation of the bacterial rotary motor [11].

The ability of the beating flagellum to respond to external forces forms the basis of the remarkable phenomenon of flagellar synchronization by mechanical coupling [12, 13]. On epithelial surfaces, collections of cilia phase-lock to a common beat frequency [2] despite active

noise [14–16]. The result are metachronal waves of coordinated cilia beating, which facilitate efficient fluid transport [17]. Pairs of flagella can synchronize their beat, *e.g.* in the bi-flagellated green alga *Chlamydomonas*, which constitutes a model system for the study of flagellar synchronization [8, 16, 18]. Here, we present a novel and versatile approach that allows us to predict the response of flagellar bending waves to external flows from recordings of their unperturbed dynamics, using *Chlamydomonas* as model system.

We first characterize how flagellar bending waves change phase speed and amplitude in response to external forces, by exposing *Chlamydomonas* cells to controlled homogeneous flows. We complement these experiments by a theoretical description of the flagellar beat as a generic limit-cycle oscillator, which may be considered a realistic analogue of previous idealized models that represented the beating flagellum by a sphere revolving around a circular orbit [19–22]. This theory, parameterized using measurements in the absence of flow, predicts deviations of perfect limit-cycle dynamics in the presence of external perturbations in quantitative agreement with experiments. Our theory further allows to computationally predict flagellar synchronization in external oscillatory flows.

Experimental setup. Single cells were held in a micropipette in a region of homogeneous flow inside a microfluidic channel, see Fig. 1(a). High-speed recordings (1 kHz) of flagellar beating were performed for different external flow velocities u , see Supplemental Material (SM) for further details [23]. For all cells analyzed, both flagella were beating in synchrony $\geq 80\%$ of the time, with a common frequency of $f_0 = 49.3 \pm 5.7 \text{ Hz}$ when no external flow was applied (mean \pm s.e., $n=6$). The shape of flagellar centerlines was tracked using custom software and is fully characterized by its tangent angle profile $\psi(s, t)$ as a function of arclength s and time t [24], see Fig. 1(b). We

limited our analysis to datasets with successful tracking of $\geq 80\%$ of the flagellar length in $\geq 80\%$ of all frames for one flagellum, corresponding to the unbiased selection of $n=6$ high-quality datasets. To illuminate the load-response of the flagellar beat during different phases of its beat, we first need to introduce the concept of flagellar phase [8, 9, 16].

Limit-cycle reconstruction. We map the periodic dynamics of the flagellar tangent angle $\psi(s, t)$ on a complex oscillator variable $Z = A \exp(i\varphi)$ with oscillator phase φ and normalized amplitude A , see Fig. 1(c), using a limit-cycle reconstruction technique [15, 25]. The logic is that in the absence of intrinsic fluctuations and external perturbations, flagellar oscillations can be characterized by a phase φ that increases at a constant rate equal to the angular frequency of the flagellar beat, $\dot{\varphi} = 2\pi f_0$, and constant amplitude $A = A_0$. In short, we used principal component analysis to express measured tangent angle profiles as superposition of two fundamental shape modes, $\psi(s, t) \approx \psi_0(s) + \beta_1(t)\psi_1(s) + \beta_2(t)\psi_2(s)$, which was followed by a normalization step that defines $Z(t)$ in terms of $Z_{\text{raw}}(t) = \beta_1(t) + i\beta_2(t)$. Specifically, we find that $Z_{\text{raw}}(t)$ jitters around a limit cycle $\bar{Z}_{\text{raw}}(\varphi)$. This limit-cycle can always be parametrized by a phase φ such that the mean phase speed is independent of φ [26]. We assign a unique phase φ to every flagellar shape by projecting its ‘shape point’ $Z_{\text{raw}}(t)$ radially onto this limit-cycle. The normalized amplitude $A = |Z_{\text{raw}}|/|\bar{Z}_{\text{raw}}|$ gauges deviations from the limit-cycle in the radial direction. Phase and amplitude allow a faithful reconstruction of waveform, see Fig. S4 in SM. We used the same set of shape modes for all data-sets: this enables a direct comparison of waveform changes among different flagella.

External flow changes speed and amplitude of flagellar oscillations. In the presence of external flow with velocity u , we observe consistent changes of flagellar bending waves. Fig. 1(d) shows the change in phase speed $\dot{\varphi}$ under external flow $u > 0$: at $\varphi = 0$ (during the effective stroke), the beat speeds up, while it slows down at $\varphi = \pi$ (recovery stroke). The recovery stroke approximately lasts $0.80\pi - 1.75\pi$ (corresponding to the part of the beat cycle, during which the center-of-mass of the flagellum moves up, relative to the long axis of the cell body). Next, for each value of the phase φ , we performed a linear regression of instantaneous phase speed versus flow velocity, $\dot{\varphi} \approx 2\pi f_0 (1 + \chi_\varphi u)$, yielding two fit parameters f_0 and χ_φ , see Fig. 1(d). We thus obtained a phase-dependent susceptibility $\chi_\varphi(\varphi)$ for the phase speed, and similarly $\chi_A(\varphi)$ for the amplitude.

Generic theory of flagellar oscillations. We present a generic theory to describe flagellar bending waves, which is independent of specific assumptions on the detailed mechanisms of motor control inside the flagellum, to predict the measured susceptibilities $\chi_\varphi(\varphi)$ and $\chi_A(\varphi)$. We build on the basic fact that regular flagellar bending waves are stable in time, *i.e.* represent a limit-cycle

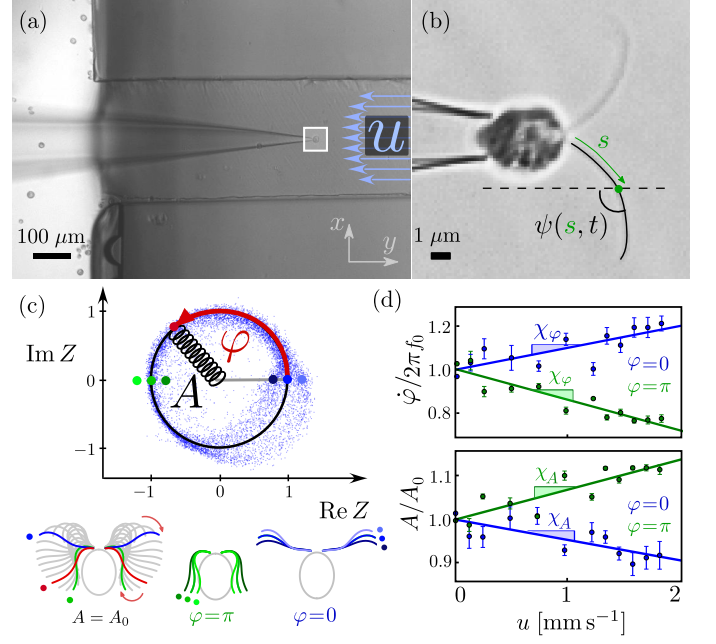


FIG. 1: *Load-response of the flagellar beat to controlled microfluidic flows.* (a) *Chlamydomonas* cell held in a micropipette exposed to flow in a microfluidic channel (velocity u at channel midline). (b) Flagellar shapes and their tangent angle profiles $\psi(s, t)$. (c) We map each flagellar shape on a shape point $Z = A \exp(i\varphi)$, see text. This defines an instantaneous phase φ and amplitude A of the flagellar beat, as well as a limit-cycle of flagellar oscillations (black) that averages out fluctuations and measurement noise. Example flagellar shapes are shown for reference shape points (colored dots). (d) Susceptibilities χ_φ and χ_A characterize the change of instantaneous phase speed and amplitude as function of external flow u . Error bars=s.e.m. for 5 sub-datasets.

oscillator. We will stick to the simple, one-dimensional case of a scalar amplitude, inline with our analysis of experimental data. Thus, we can describe flagellar dynamics of a *Chlamydomonas* cell by a minimal number of degrees of freedom. We delimit ourselves to the particularly simple case of perfectly symmetric beating. Thus, for a freely swimming cell, the phase space vector reads $\mathbf{q} = (\varphi, A, y)$. Here, φ and A denote phase and amplitude of the flagella, while y denotes the position of the cell body center, where we chose the y -axis parallel to the long axis of the cell body, see Fig. 1(a,b). By symmetry, the cell swims along the y -direction.

We now derive equations of motion for the swimming cell from a balance of forces between active flagellar driving forces $Q_j(\varphi)$ and friction forces $P_j(\varphi)$, using a general framework of Lagrangian mechanics for dissipative systems [27]. The total rate of dissipation \mathcal{R}_{tot} of the system consisting of flagella and surrounding fluid can be written as

$$\mathcal{R}_{\text{tot}} = \mathbf{P} \cdot \dot{\mathbf{q}} = P_\varphi \dot{\varphi} + P_A \dot{A} + P_y \dot{y}, \quad (1)$$

where the generalized friction forces P_j are conjugate

to the generalized velocities \dot{q}_j , $j \in \{\varphi, A, y\}$. For example, $P_\varphi \dot{\varphi}$ would be the rate of dissipation associated with advancing both flagella in the beat cycle at speed $\dot{\varphi}$, while keeping all other degrees of freedom fixed. Friction forces will comprise both a contribution from hydrodynamic friction of the surrounding viscous fluid, as well as possibly internal friction inside the beating flagella.

Any flagellar dynamics will set the surrounding fluid in motion, and will thus induce viscous dissipation. In the overdamped regime of low Reynolds number, applicable to cellular swimmers [28], hydrodynamic friction forces are linearly related to the velocities, *i.e.* $\mathbf{P}^{(h)} = \mathbf{\Gamma}^{(h)} \cdot \dot{\mathbf{q}}$. The hydrodynamic friction matrix $\mathbf{\Gamma}^{(h)}(\mathbf{q})$ can be calculated by solving the Stokes equation with boundary conditions on the surface of the swimmer specified by \mathbf{q} and $\dot{\mathbf{q}}$; Fig. 2(a) shows an example with $\mathbf{q} = (\pi, 1, 0)$ and $\dot{\mathbf{q}} = (2\pi f_0, 0, u)$. In principle, these generalized friction forces can be computed for any beat pattern parameterized by phase φ and amplitude A . Here, we employ the beat pattern shown in Fig. 1(c) and a fast boundary element method [29, 30]. As technical side-note, in simulations involving large flow velocities (*e.g.* for flagellar stalling studied below) the range of the flagellar amplitude was constrained to account for steric interactions between flagella and cell body.

In addition to hydrodynamic dissipation in the surrounding fluid, energy is also dissipated inside the beating flagellum itself. This intraflagellar friction combines effects of incomplete energy conversion by molecular motors and possibly dissipation by viscoelastic structural elements in the flagellar axoneme such as nexin linkers. In the absence of detailed knowledge on this intraflagellar friction, we make the simple ansatz of a rate of intraflagellar dissipation $\mathcal{R}^{(i)}$ proportional to the total dissipation rate

$$\mathcal{R}^{(i)} = (1 - \eta)\mathcal{R}_{\text{tot}}. \quad (2)$$

Here, η represents an efficiency of chemo-mechanical energy conversion. The total friction matrix can then be written as $\Gamma_{ij} = \Gamma_{ij}^{(h)}/\eta$, with $i, j \in \{\varphi, A\}$ and the total friction forces read $\mathbf{P} = \mathbf{\Gamma} \cdot \dot{\mathbf{q}}$.

The equation of motion of flagellar dynamics is specified by a balance of generalized forces

$$Q_\varphi = P_\varphi \text{ and } Q_A = P_A, \quad (3)$$

where the active driving forces Q_φ and Q_A conjugate to φ and A coarse-grain active motor dynamics inside the flagellum, see also Fig. 2(b). Below, we calibrate these active driving forces using measured limit-cycle dynamics in the absence of flow. The force P_y conjugate to y corresponds to the y -component of the total force acting on the cell. For a freely swimming cell, $P_y=0$. For a clamped cell, y is constant and P_y represents the constraining force required to ensure this constraint. The case of an external flow with constant velocity u is incorporated in this formalism by setting $\dot{y} = u$.

By convention, the unperturbed limit-cycle dynamics of the flagellar beat for $u = 0$ is characterized by $\dot{\varphi} = 2\pi f_0$ and $A = A_0$. This requirement uniquely determines $Q_\varphi(\varphi)$ and $Q_A(\varphi, A)$ for $A = A_0$, as $Q_\varphi(\varphi) = \Gamma_{\varphi\varphi}(\varphi, A_0)2\pi f_0$ and $Q_A(\varphi, A_0) = \Gamma_{A\varphi}(\varphi, A_0)2\pi f_0$. Next, we extend the domain of definition of Q_A to the case $A \neq A_0$ by making the simple ansatz of an effective amplitude spring acting on $A - A_0$

$$Q_A(\varphi, A) = Q_A(\varphi, A = A_0) - k_A(\varphi)(A - A_0). \quad (4)$$

This amplitude spring with spring constant k_A ensures the stability of flagellar limit-cycle oscillations with respect to amplitude perturbations, which has been observed experimentally [9]. In a simple phenomenological description, amplitude perturbations decay with a characteristic relaxation time τ_A , $\tau_A \dot{A} = A_0 - A$. For simplicity, we assume that τ_A does not depend on phase φ . A value of $\tau_A = 5.9$ ms has been previously determined by a measurement of the correlation time of amplitude fluctuations [15]. Equation (4) uniquely specifies a choice for the phase-dependent amplitude stiffness $k_A(\varphi)$, see SM. All quantities in our theoretical description of flagellar limit-cycle dynamics are now calibrated, except for the unknown flagellar efficiency parameter η , where we used only beat patterns measured in the absence of external flow. Next, we compare theory and experiment for the load-response of flagellar oscillations in the presence of external flow, and determine η by a simple fit.

The load-response of the beating flagellum. We characterize the load-response of the flagellar beat to external flow in terms of phase-dependent susceptibilities $\chi_\varphi(\varphi)$ and $\chi_A(\varphi)$ for phase speed and amplitude, respectively, as introduced already in Fig. 1(d). An average of χ_φ for $n=6$ cells is shown in Fig. 2(c), revealing a reproducible response of flagellar bending waves to external flow. During the effective stroke ($\varphi \approx 0$), we observe an increase in phase speed ($\chi_\varphi > 0$), whereas the recovery stroke slows down ($\chi_\varphi < 0$ for $\varphi \approx \pi$). These two effects partially cancel, resulting in a net change of the beat frequency by a few percent only, see also Fig. 2(d). Our analysis highlights the importance of a sub-cycle analysis of the flagellar load-response. For the amplitude, we find $\chi_A > 0$ for $\varphi \approx \pi$, *i.e.* the flagella are closer to the cell body during the recovery stroke. Our simple theory captures the principal features of the experimentally determined phase-dependence, yet not all details can be reproduced. A one-parameter fit provides an estimate for the flagellar efficiency parameter η , yielding $\eta = 0.21 \pm 0.06$ (mean \pm s.e., $n=6$). The flagellar susceptibilities used to estimate η are robust with respect to uncertainty in τ_A or using a different waveform, see Figs. S5 and S6 in SM.

Stalling of flagellar oscillations. For strong external flow, we find that the recovery stroke slows down both in theory and experiment – up to a point, where the flagellar beat comes to a halt. While increasing flow velocity u in experiments, we consistently observed first a

slight increase of beat frequency f , followed by a rapid decrease; two generic cases are shown in Fig. 2(d). Above a critical flow velocity u_c , the flagellar beat arrests in the recovery stroke. Upon decreasing u , flagella reproducibly resumed regular beating. Occasionally, a slight hysteresis was noticeable, see *e.g.* Fig. 2(d)-①. In 10 out of 16 *cis*-flagella (yet not in *trans*-flagella), we observed a different, non-planar mode of flagellar beating with distinctly different frequency for intermediate values of u , see *e.g.* Fig. 2(d)-② and Supplemental Movie S1. Otherwise, we did not observe significant differences in the load-response of *cis*- and *trans*-flagella. For negative flow velocities, the flagellar beat stalls already at $u \approx -0.5$ mm/s, see *e.g.* Fig. 2(d)-③ and Supplemental Movie S2.

Our simple theory predicts a similar dependence of beat frequency f on flow velocity for $u > 0$, with stalling at a critical flow velocity $u_c = 14$ mm s⁻¹, see Fig. 2(d). This flagellar stalling displays characteristic signatures of a saddle-node bifurcation. Intriguingly, our simple theory predicts flagellar stalling for $u > 0$ much better than for $u < 0$, when stalling occurs during the effective stroke, characterized by low flagellar curvature. Flagellar curvature has been previously proposed as key determinant of flagellar motor control [31, 32]. We anticipate that flagellar load-responses and stalling can provide a test case for refined theories of flagellar beating [24, 31–34].

Flagellar phase-locking to external driving. Recent experiments by Quaranta *et al.* demonstrated phase-locking of *Chlamydomonas* flagellar beating to external oscillatory fluid flow [35]. In accordance, our theory predicts similar phase-locking, see Fig. 3. The width of the resultant Arnold tongue agrees with measurements from [35] within 20% (using $\eta = 0.2$). Naturally, this flagellar synchronization relies on the fact that beating flagella respond to changes in hydrodynamic load. The width of the Arnold tongue would approach zero for $\chi_\varphi = \chi_A = 0$, *i.e.* for a flagellum with vanishing energy efficiency $\eta = 0$. On the other hand, assuming maximal efficiency $\eta = 1$ would result in an Arnold tongue that is too wide to account for the experimental observations. Likewise, synchronization of *cis*- and *trans*-flagellum depend on flagellar load-responses [8, 16]; for this, phase-dependent driving forces and non-isochrony of flagellar oscillations (see Figs. S3 and S8 in SM) are relevant [20, 21].

Discussion. We report direct measurements of dynamic load-responses in an evolutionary conserved motor system, the beating flagellum. We characterized the flagellar beat as a limit-cycle oscillator that displays characteristic phase and amplitude susceptibilities in response to an external force. Motivated by this description, we formulated a theory of flagellar dynamics in terms of a phase-amplitude oscillator, which is calibrated by experimental data in the absence of external flow. This minimal theory, based on the assumption of small perturbations of flagellar limit cycle oscillations, is able to predict key fea-

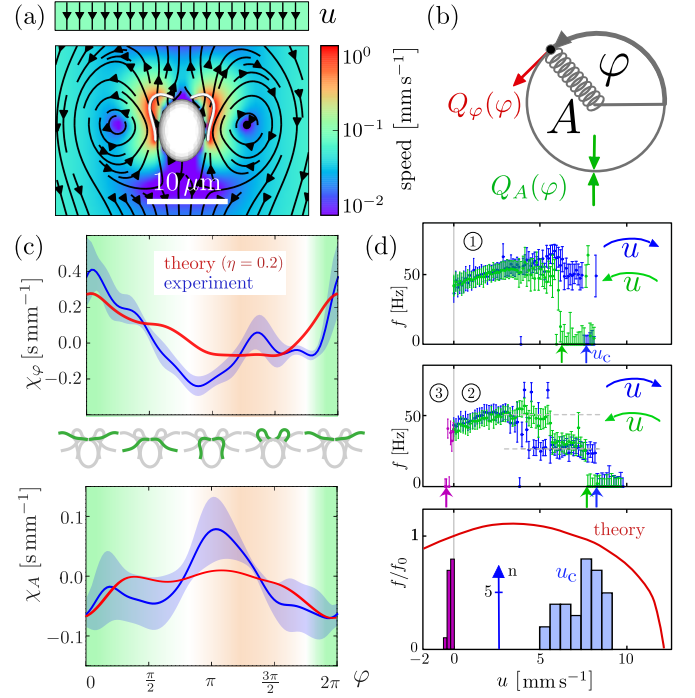


FIG. 2: *Theory and experiment of flagellar load-response.* (a) We computed hydrodynamic friction forces acting on a beating flagellum numerically by solving the Stokes equation for viscous flow. (b) We introduce a generic theoretical description of flagellar oscillations as a limit-cycle oscillator with phase φ and amplitude A . An active flagellar driving force Q_φ coarse-grains active motor dynamics inside the flagellum. A constraining force Q_A for the amplitude ensures stability of the limit-cycle. These phase-dependent active forces are uniquely calibrated from experimental data in the absence of flow. (c) Phase-dependent susceptibilities χ_φ and χ_A for phase speed and amplitude, respectively. Comparison of experiment (blue, mean \pm s.e.) and theoretical prediction (red) yields $\eta = 0.21 \pm 0.06$ (mean \pm s.e., $n=6$) for the energy efficiency of the flagellar beat. The duration of effective and recovery stroke are indicated by green and red shading, respectively. (d) External flow induces stalling of flagellar oscillations beyond a critical flow velocity u_c . *Top, middle:* typical frequency responses for three flagella, numbered 1,2,3. *Bottom:* theory prediction of frequency response and stalling (red); inset: histograms of experimentally measured u_c ($u > 0$: blue, $n=33$ flagella, $u < 0$: lilac, $n=16$ flagella).

tures of the flagellar load-response, such as acceleration of the effective stroke and deceleration of the recovery stroke by external flow, as well as reversible stalling of flagellar oscillations beyond a critical flow velocity, in quantitative agreement with experiment. Details of the phase-dependent load-response, hysteresis of flagellar stalling, switching to a second, non-planar mode of beating, as well as stalling at surprisingly small negative flow velocities, are not accounted for by our simple theory, yet may be informative for refined theories of flagellar beating and the underlying dynamics of molecular motors [24, 31–34].

By comparison of theory and experiment, we obtained

an estimate $\eta = 0.21 \pm 0.06$ for the energy efficiency of the flagella beat, defined as the ratio of mechanical work performed by the beating flagellum on the surrounding fluid divided by the chemical energy input required to sustain its beat. Previous estimates for η reported values in the range $\eta = 0.1 - 0.4$ [36–39], see also SM. In our theory, we assume an active flagellar driving force that is independent of external load. This assumption is consistent with recent experiments, which show that flagellar ATP consumption is rather insensitive to beat frequency and mechanical load [39]. Accordingly, any increase in load is compensated by a reduction in speed, not an increase in fuel consumption.

The load-response of beating flagella reported here is an essential prerequisite for flagellar synchronization by mechanical coupling, [40], without which hydrodynamic synchronization would be impossible.

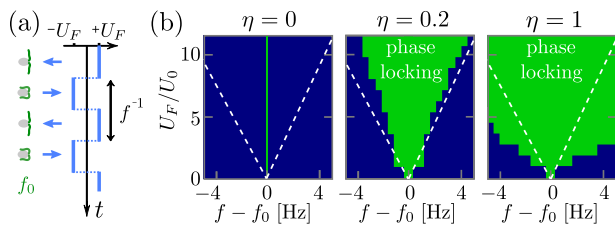


FIG. 3: Phase-locking of *Chlamydomonas* flagellar beat to external oscillatory flow. (a) Sketch of original experiment [35]. (b) Computed Arnold tongues as function of flow frequency f and amplitude U_F for different values of the flagellar energy efficiency η . Dashed lines indicate the phase-locking region measured in [35]. Parameters: $U_0 = 0.11 \text{ mm s}^{-1}$, $f_0 = 50 \text{ Hz}$ intrinsic frequency of flagellar beat.

G.S.K. and B.M.F. acknowledge financial and institutional support from the German Science Foundation “Microswimmers” priority program SPP 1726 (Grant No. FR 3429/1-1). We thank E. Terriac for help with design and fabrication of microfluidic chips and useful discussions. G.S.K and C.R. contributed equally to this work.

* Electronic address: benjamin.m.friedrich@tu-dresden.de

[1] J. Gray, *Ciliary Movements* (Cambridge Univ. Press, Cambridge, 1928).
[2] M. Sanderson and M. Sleight, *J. Cell Sci.* **47**, 331 (1981).
[3] W. C. Worthington and R. S. Cathcart, *Science* **139**, 221 (1963).
[4] Z. Carvalho-Santos, J. Azimzadeh, J. B. Pereira-Leal, and M. Bettencourt-Dias, *J. Cell Biol.* **194**, 165 (2011).
[5] D. Nicastro, C. Schwartz, J. Pierson, R. Gaudette, M. E. Porter, and J. R. McIntosh, *Science* **313**, 944 (2006).
[6] C. Brokaw, *J. exp. Biol.* **45**, 113 (1966).
[7] C. Brokaw, *J. exp. Biol.* **62**, 701 (1975).
[8] V. F. Geyer, F. Jülicher, J. Howard, and B. M. Friedrich, *Proc. Natl. Acad. Sci. U.S.A.* **110**, 18058 (2013).

[9] K. Y. Wan and R. E. Goldstein, *Phys. Rev. Lett.* **113**, 238103 (2014).
[10] A. J. Hunt, F. Gittes, and J. Howard, *Biophys. J.* **67**, 766 (1994).
[11] X. Chen and H. C. Berg, *Biophys. J.* **78**, 1036 (2000).
[12] G. I. Taylor, *Proc. Roy. Soc. Lond. A* **209**, 447 (1951).
[13] D. R. Brumley, K. Y. Wan, M. Polin, and R. E. Goldstein, *eLife* **3**, e02750 (2014).
[14] M. Polin, I. Tuval, K. Drescher, J. P. Gollub, and R. E. Goldstein, *Science* **325**, 487 (2009).
[15] R. Ma, G. S. Klindt, I. H. Riedel-Kruse, F. Jülicher, and B. M. Friedrich, *Phys. Rev. Lett.* **113**, 048101 (2014).
[16] R. E. Goldstein, M. Polin, and I. Tuval, *Phys. Rev. Lett.* **103**, 168103 (2009).
[17] J. Elgeti and G. Gompper, *Proc. Natl. Acad. Sci. U.S.A.* **110**, 4470 (2013).
[18] U. Ruffer and W. Nultsch, *Cell Motil. Cytoskel.* **7**, 87 (1987).
[19] A. Vilfan and F. Jülicher, *Phys. Rev. Lett.* **96**, 58102 (2006).
[20] T. Niedermayer, B. Eckhardt, and P. Lenz, *Chaos* **18**, 037128 (2008).
[21] N. Uchida and R. Golestanian, *Phys. Rev. Lett.* **106**, 058104 (2011).
[22] B. M. Friedrich and F. Jülicher, *Phys. Rev. Lett.* **109**, 138102 (2012).
[23] See Supplemental Material, which includes Refs. [41–43].
[24] I. H. Riedel-Kruse, A. Hilfinger, J. Howard, and F. Jülicher, *HFSP J.* **1**, 192 (2007).
[25] S. Werner, J. C. Rink, I. H. Riedel-Kruse, and B. M. Friedrich, *PloS one* **9**, e113083 (2014).
[26] B. Kralmann, L. Cimponeriu, M. Rosenblum, A. Pikovsky, and R. Mrowka, *Phys. Rev. E* **77** (2008).
[27] K. Poltsek and B. M. Friedrich, *New J. Phys.* **15**, 045005 (2013).
[28] E. Lauga and T. R. Powers, *Rep. Progress Phys.* **72**, 096601 (2009).
[29] Y. Liu and N. Nishimura, *Engineering Analysis with Boundary Elements* **30**, 371 (2006).
[30] G. S. Klindt and B. M. Friedrich, *Phys. Rev. E* **92**, 063019 (2015).
[31] C. J. Brokaw, *J. exp. Biol.* **55**, 289 (1971).
[32] P. Sartori, V. F. Geyer, A. Scholich, F. Jülicher, and J. Howard, *eLife* **5**, e13258 (2016).
[33] C. B. Lindemann, *J. Theoret. Biol.* **168**, 175 (1994).
[34] S. Camalet and F. Jülicher, *New J. Phys.* **2**, 24 (2000).
[35] G. Quaranta, M.-E. Aubin-Tam, and D. Tam, *Phys. Rev. Lett.* **115**, 238101 (2015).
[36] C. Brokaw, *Science* **156**, 76 (1967).
[37] Y. Katsu-Kimura, F. Nakaya, S. A. Baba, and Y. Mogami, *J. exp. Biol.* **212**, 1819 (2009).
[38] R. A. Cardullo and J. M. Baltz, *Cell Motil. Cytoskel.* **19**, 180 (1991).
[39] D. T. Chen, M. Heymann, S. Fraden, D. Nicastro, and Z. Dogic, *Biophys. J.* **109**, 2562 (2015).
[40] B. M. Friedrich, *Eur. Phys. J. Special Topics* **225**, 2353 (2016).
[41] D. S. Gorman and R. Levine, *Proc. Natl. Acad. Sci. U.S.A.* **54**, 1665 (1965).
[42] K. C. Leptos, K. Y. Wan, M. Polin, I. Tuval, A. I. Pesci, and R. E. Goldstein, *Phys. Rev. Lett.* **111**, 158101 (2013).
[43] *MatPIV v1.6.1*, <http://www.math.uio.no/~jks/matpiv>.